ACS APPLIED MATERIALS & INTERFACES

Research Article

www.acsami.org

Prediction of the Active Layer Nanomorphology in Polymer Solar Cells Using Molecular Dynamics Simulation

Ali Reza Ashrafi Khajeh,[†] Karthik Shankar,[‡,§] and Phillip Choi*[,†]

[†]Department of Chemical and Materials Engineering and [‡]Department of Electrical and Computer Engineering, University of Alberta, Edmonton, Alberta T6G 2 V4

[§]National Institute for Nanotechnology, National Research Council, 11421 Saskatchewan Drive, Edmonton, AB, T6G 2M9, Canada

Supporting Information

ABSTRACT: Active layer nanomorphology is a major factor that determines the efficiency of bulk heterojunction polymer solar cells (PSCs). Synthesizing diblock copolymers in which acceptor and donor materials are the constituent blocks is the most recent method to control the structure of the active layer. In the current work, a computational method is proposed to predict the nanomorphology of the active layer consisting of a diblock copolymer. Diblock copolymers have a tendency to self-organize and form well-defined nanostructures. The shape of the structure depends on the Flory–Huggins interaction parameter (i.e., χ), the total degree of polymerization (N) and volume fractions of the constituent blocks (φ_i). In this work, molecular dynamics (MD) simulations were used to calculate χ parameters for two different block copolymers used in PSCs: P3HT-*b*-poly(S_8A_2)-C_{60} and P3HT-*b*-poly(n-butyl acrylate-*stat*-acrylate perylene) also known as P3HT-*b*-PPerAcr. Such calculations indicated strong segregation of blocks into cylindrical structure for P3HT-*b*-poly(S_8A_2)-C_{60} and intermediate segregation into cylindrical structure for P3HT-*b*-PPerAcr. Experimental results of P3HT-*b*-poly(S_8A_2)-C_{60} and P3HT-*b*-PTP4AP, a diblock copolymer having very similar structure to P3HT-*b*-PPerAcr, validate our predictions.

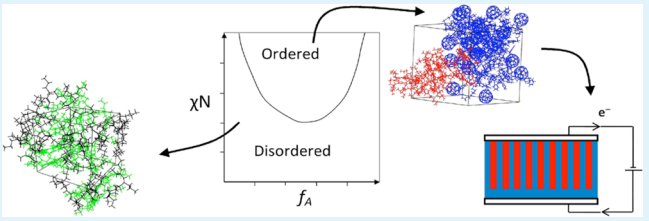

KEYWORDS: *active layer, diblock copolymers, nanomorphology, molecular dynamics simulation, Flory–Huggins interaction parameter*

1. INTRODUCTION

Environmental issues related to energy production from fossil fuels[1] and soaring crude oil prices in the past decade have been the main stimulants for the development of renewable energy resources. More energy from sunlight strikes Earth in 1 h than all of the energy consumed by humans in an entire year,[2] and finding a cost-efficient way to capture it can solve energy concerns of the human race for the foreseeable future.

To obtain the highest efficiency in the polymer solar cells, the thickness of the active layer must be greater than 240 nm, whereas the size of the acceptor and donor domains ought to be in the 5–20 nm range.[3,4] It is noteworthy that the main breakthroughs in the efficiency of polymer solar cells in the past two decades occurred because of the fundamental changes in the morphology of the active layer through introduction of diffused bilayer[5] and bulk heterojunction architectures for the active layer. Bulk heterojunction (BHJ) morphology in which acceptor and donor materials are completely mixed in the active layer is the most suitable structure for optimal charge separation. However, in the BHJ active layer, materials must form ordered and continuous phases to yield high charge collection efficiencies.

Several methods have been developed to improve the morphology of the active layer in BHJ solar cells through thermal treatment,[6−9] solvent annealing,[10,11] additives,[12,13] etc. All these methods require extra processing steps and hence increase the embedded energy, cost and complexity of the solar cells. Furthermore, these methods are not generic and yield higher efficiencies only for specific active layer materials.

Using diblock copolymers with acceptor and donor blocks is the newest approach to attain the desired nanomorphology in the active layer. Block copolymers are macromolecules composed of sequences or blocks of chemically distinct repeat units.[14] Upon blending of two thermodynamically incompatible homopolymers, they tend to form macroscopic domains of pure polymers. However, in the case of block copolymers, because of the covalent bond between separate blocks, they cannot separate to form macro-domains. The size of block copolymer domains depend on the chain lengths of the blocks. Diblock copolymers in the active layer, because of their tendency to self-segregate, do not need extra processing steps to attain a suitable nanomorphology and therefore are promising candidates for future PSCs.

Currently, the field of organic photovoltaics is dominated by active layers composed of small molecule-small molecule or small molecule-semiconducting polymer blends. First, the nanoscale self-segregation tendency of diblock copolymers that consist of at least one absorbing, π-conjugated block may

Received: July 16, 2012
Accepted: May 9, 2013
Published: May 9, 2013

   dx.doi.org/10.1021/am400566f | ACS Appl. Mater. Interfaces 2013, 5, 4617–4624

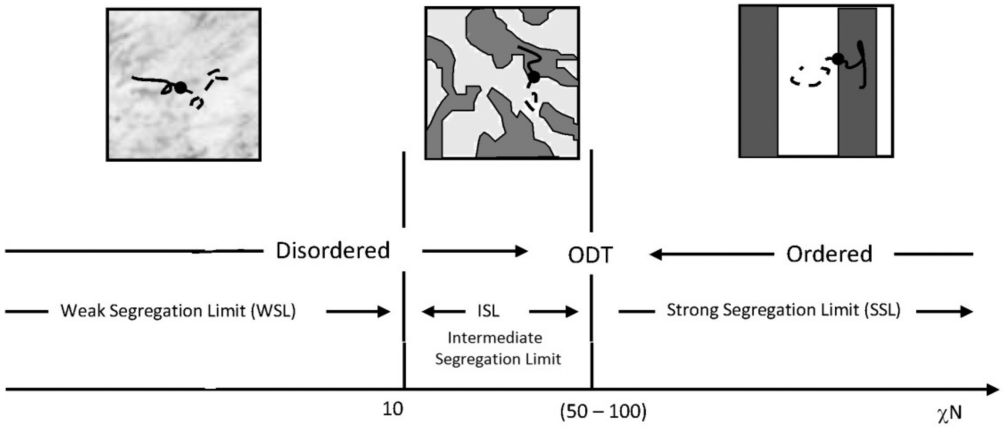

Figure 1. Illustration of the different states of segregation in diblock copolymers.

be used to achieve ordered heterojunctions by selectively etching away the nonconjugated block and filling the vacant spaces with a suitable π-conjugated small molecule or polymer using a solvent orthogonal to the conjugated block. Second, despite advantages such as enhanced processability, absorption of both components contributing to better light harvesting, potentially longer charge collection paths and higher potential stability, active layers consisting of conjugated polymer–polymer blends have performed poorly thus far in comparison to polymer-small molecule blends, primarily because of difficulties in engineering the correct nanomorphology of the active layer. In this context, the self-segregation tendency of diblock copolymers is particularly interesting as a method to overcome the morphology limitation of polymer–polymer blends for PSCs.

A two-step process is usually followed to design new materials for PSCs. First, an acceptor–donor pair must be designed which has suitable optoelectronic properties. The second step is to synthesize the suggested materials and fabricate a solar cell to evaluate the morphology and efficiency attained using new materials. New material synthesis and characterization is very cumbersome and requires considerable amount of time, knowledge, and budget. Moreover, because of the sensitivity of polymer solar cells to ambient, duration of light exposure, contact electrode degradation, and processing conditions, the fabrication and performance evaluation of optimized solar cells is a delicate and multidisciplinary process.

Although optoelectronic properties, charge mobility, and absorption spectra of the acceptor and donor materials are important factors in determining the performance of the solar cells, the efficiency of the solar cell will be low if the active layer does not have proper nanomorphology even if the other properties of the active layer materials are superior. The importance of the active layer nanomorphology in the performance of solar cells has been discussed extensively elsewhere.[15−21] Finding a computational method to evaluate nanomorphology of the active layer can save a tremendous amount of time and investment. In the current work, we present a molecular dynamics (MD) method to predict the nanomorphology of the block copolymers commonly used in the PSCs. Here, we would like to point out that although there has been an explosion in papers on organic solar cells employing primarily an empirical approach toward engineering the active layer morphology, papers that employ the modeling/simulation approach to predict the morphology are scarce. It is only in the very recent literature that researchers have reported the use of computer simulation techniques to address issues related to polymer solar cells. For instance, Do et al.[22] performed molecular dynamics simulation of P3HT and PBTTT to provide a rationale for higher hole mobility in PBTTT versus P3HT. They performed coarse-grained MD simulations of pure P3HT and PBTTT and used pair distribution function analysis of inter- and intrachain site pairs to propose a more highly ordered morphology in PBTTT versus P3HT as the reason of better charge mobility in PBTTT. In another work, Lee et al.[23] performed multiscale MD simulation to reproduce phase behavior of P3HT and PCBM blend. It is worth noting that the segregation of acceptor–donor material in PSC active layer is kinetic-driven and a MD simulation of at least several milliseconds is required to equilibrate the system in order to reproduce its phase nanomorphology. And this requires very high computational cost. In the present work, we will use an approach different from that of Lee et al. to determine the phase nanomorphology. In particular, we will use the rotational isomeric state model to generate the initial conformations of the polymers of interest and will equilibrate them using MD simulation. The corresponding Flory–Huggins interaction parameters will then be calculated and used for the determination of the phase behavior of the systems. In our view, this approach is computationally more cost-effective.

2. THEORETICAL BACKGROUND

The morphology of AB diblock copolymer has been the subject of comprehensive theoretical[24,25] and experimental[26,27] studies and its behavior is relatively well understood. The morphology of undiluted diblock copolymers is determined by three factors: the A–B segment–segment Flory–Huggins interaction parameter (χ), the volume fractions of constituent blocks in the polymer (φ_A and φ_B) and the overall degree of polymerization (N).

Phase diagrams of diblock copolymers are divided into three regimes: weak segregation limit (WSL), intermediate segregation region (ISR) and strong segregation limit (SSL) depending on the combined parameter, χN.[28] In the WSL, the composition in different regions deviates slightly from the average value. This means that we do not have domains of pure A or B blocks and the two blocks are intimately mixed at the microscopic level.[29] For copolymers with infinite length ($N\rightarrow\infty$), as the χN value approaches 10, individual chains are

significantly extended from their unperturbed Gaussian dimensions which are considered as a signal for crossover from WSL to ISR.[30] As the χN value approaches roughly 50–100,[28] domains of pure blocks with sharp interfaces start to appear, which is the characteristic of the SSL. Three regimes in block copolymer phase behavior are schematically illustrated in Figure 1.

Fredrickson and Helfand[31] formulated order–disorder transition χN as a function of the degree of polymerization for symmetric diblock copolymers with a finite degree of polymerization

$$(\chi N)_{\mathrm{ODT}} = 10.495 + 41.0\bar{N}^{-1/3} \quad (1)$$

where $\bar{N} = Na^6\nu^{-2}$ and a and ν are the statistical segment length and volume, respectively.

Flory–Huggins interaction parameter decreases with increasing temperature and in many cases, χ exhibits a linear reciprocal dependence on temperature

$$\chi \approx \alpha T^{-1} + \beta,\ \alpha > 0 \quad (2)$$

Block copolymers can form various structures in the strong segregation limit depending on the volume fraction of the constituent blocks. A typical phase diagram is shown in Figure 2. Spherical structure is observed when the volume fraction of one block is much less than the other block. This type of nanostructure is not suitable for PSC active layer and this region should be avoided. As the volume fraction of the block increases, cylindrical, bicontinuous, perforated, and lamellar structures appear. Cylindrical, bicontinuous and lamellar structures are suitable for our purpose but the perforated structure must be avoided since the formed domains are not continuous. It must be noted that the phase diagram is not generic in a sense that the volume fractions corresponding to the phase boundaries depend on the chemical composition of the block copolymer but different block copolymers exhibit similar phase diagram (i.e., they will exhibit similar nanostructures over comparable volume fraction ranges).

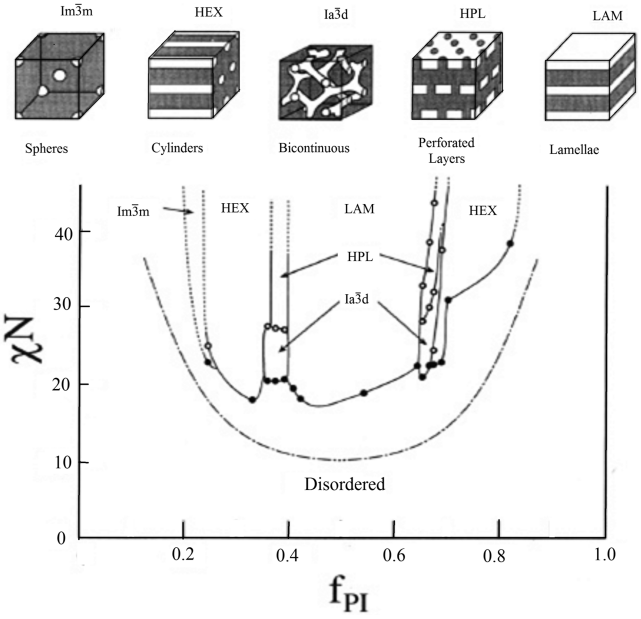

Figure 2. Upper panel shows five different common nanostructures and phase diagram of polyisoprene-polystyrene is shown in lower panel. f_{PI} is the volume fraction of polyisoprene. Reprinted with permission from ref 32. Copyright 1995 American Chemical Society.

Because the volume fraction of blocks and the overall degree of polymerization can be readily controlled while synthesizing the block copolymer, the most important factor that determines nanostructure and degree of self-segregation is the Flory–Huggins interaction parameter. Finding suitable A and B blocks that have the proper χ parameter value and proper optoelectronic properties is the most important step in the design of a copolymer that will form the desired nanomorphology and hence will yield a higher power conversion efficiency.

It is noteworthy that the phase diagram of a diblock copolymer gives the nanomorphology of the diblock copolymer phase at thermodynamic equilibrium. However, in the fabrication of polymer solar cells, the active layer molecules do not have enough time to reach equilibrium conformations in most cases. Hence, the phase segregation shown in Figure 2 corresponds to the highest achievable segregation under the given experimental conditions. However, conditions closer to equilibrium are achieved in subsequent solvent annealing steps. The equilibrium configuration is also important for understanding the stability of the nanomorphology of the active layer during device operation.

An acceptor–donor pair with a χ value larger than 100 will lie in the SSL limit. There are two advantages for a system that exhibits characteristics of SSL: first, pure domains of acceptor and donor material provide better light absorption and lower trap densities. Second, extended and straighter polymer backbone means that the charge collection route is shorter and both geminate and bimolecular recombination are less likely to occur.

There are two different approaches to calculate the χ parameter: the first method uses Hildebrand solubility parameters to calculate the χ parameter while in the second method, lattice theory is used to derive an expression for the χ parameter. These methods are described extensively elsewhere.[33] In the current work, lattice theory is used from which the following expression can be derived for the Flory–Huggins parameter:[34]

$$\chi = \frac{\Delta E_{mix}}{RT\varphi_A\varphi_B} \quad (3)$$

where $\Delta E_{\mathrm{mix}} = E_{\mathrm{blend}} - E_{\mathrm{A}} - E_{\mathrm{B}}$ is the potential energy of mixing, R is the ideal gas constant, T is the temperature, and φ_i is the volume fraction of species i.

In general, ΔE_{mix} is small in comparison to the energies of the individual E_{i} values. This is the drawback of this method as the calculated χ value tends to carry a relatively large uncertainty. Despite this drawback, this work demonstrates that such an approach yields reasonable prediction of the nanomorphology for two diblock copolymers used in the active layer of PSCs.

3. SIMULATION METHOD

All MD simulations were performed using the Materials Studio software package. (MS Modeling version 4.0, Accelrys)

The COMPASS force field[35] was used throughout the work to describe bonded and nonbonded interactions. In this force field

$$E = E_{\mathrm{b}} + E_{\theta} + E_{\varphi} + E_{\chi} + E_{\mathrm{nonbound}} + E_{\mathrm{cross\text{-}coupling}} \quad (4)$$

The first four terms represent bonded interactions that correspond to the energy associated with bond stretching (E_{b}), bond angle bending

(E_θ), torsion angle rotations (E_φ), and Wilson out-of-plane angle (E_χ). The nonbonded term represents interactions consisting of Lennard–Jones (LJ) 9–6 function for the van der Waals interactions and the Coulombic function for the electrostatic interactions. The nonbonded term is used for interactions between pairs of atoms that are separated by two or more intervening atoms or those that belong to different molecules. The cross-coupling term is used for the prediction of vibration frequencies and structural variations associated with conformational changes.

On the basis of first principle quantum mechanical calculations, the partial atomic charges on the molecules were preset by the COMPASS force field. The electrostatic interaction was calculated using the Ewald summation method because it provides a more effective way of handling long-range interactions.[36]

3.1. Construction of Liquid-State Models. To reduce the equilibration time to obtain equilibrium structure, the initial amorphous structures of the individual blocks of the block copolymers of interest were constructed using the rotational isometric state (RIS) model.[37−39] In the RIS model, there are only a few torsional angles accessible to each chemical bond. And the probability profile of torsion angles depends on their energy level and temperature. The details of determining the RISs of a polymer are described elsewhere.[33]

The amorphous cell construction process starts by placing the atom in the middle of the polymer of interest in a random place inside the box and then grows segments with a stepwise process using known values of bond lengths, bond angles and torsion angles. It is worth noting that having a range of possible RISs facilitates the amorphous cell construction as it gives more freedom in growing chains around obstacles. An initial density of 0.5 g/cm^3 was used to construct the amorphous cells and isothermal–isobaric (i.e., NPT) MD simulations were used to compress the cell to its actual density. Figure 3 shows the resultant structures of the simulation cell after NPT simulations. It should be noted that the blocks shown in the figure are not connected. This is required in the context of the Flory–Huggins theory. In this study, one molecule of each polymer block of interest was built in the amorphous cell. Three-dimensional periodic conditions were used. The introduction of periodic boundary conditions is equivalent to modeling the polymers in the bulk state.

3.2. Molecular Dynamics Simulation. The initial amorphous cell is usually in high energy state. Energy minimization was performed on the systems to remove van der Waals overlaps. The minimization was carried out with the steepest descent method, followed by the conjugate gradient method and ended with a Newton method. Velocities of atoms for the initial trajectory of each simulation are generated randomly using Boltzmann distribution.

NPT simulations were used to compress the cell to its equilibrium volume to obtain its density. In these simulations, number of molecules in the cell, pressure, and temperature were kept constant while volume of the cell changed. All NPT simulations were carried out in the atmospheric pressure (0.0001 GPa). NPT simulations ought to be carried out until the density of the system is stabilized. In the case of NPT simulations, there is not a module to monitor the density of the system during the run so NPT simulations were performed in several intervals and the average density was evaluated after each interval. These runs were continued until the difference between the densities in consecutive steps was less than 0.4%. Simulation time for NPT runs are reported in Table 1 in the Supporting Information. Berendsen thermostat and barostat[33] were used to keep temperature and pressure constant.

NVT simulations were used to calculate the potential energy of the system. In these simulations, the number of molecules in the cell, volume and temperature are kept constant. NPT ensemble was not used to calculate potential energy for two reasons: first based on the lattice theory, the volume of the simulation cell must be kept constant. And higher computational speed is the second reason. In NVT ensemble, temperature is the only controllable value but both pressure and temperature must be controlled in NPT ensembles. Berendsen thermostat[40] was used to keep temperature constant. The cell volume was calculated using the equilibrium density obtained from NPT simulations at the same temperature. NVT simulations were carried out until the potential energy of the system was stabilized. Simulation time for NVT runs are reported in Table 1 in the Supporting Information.

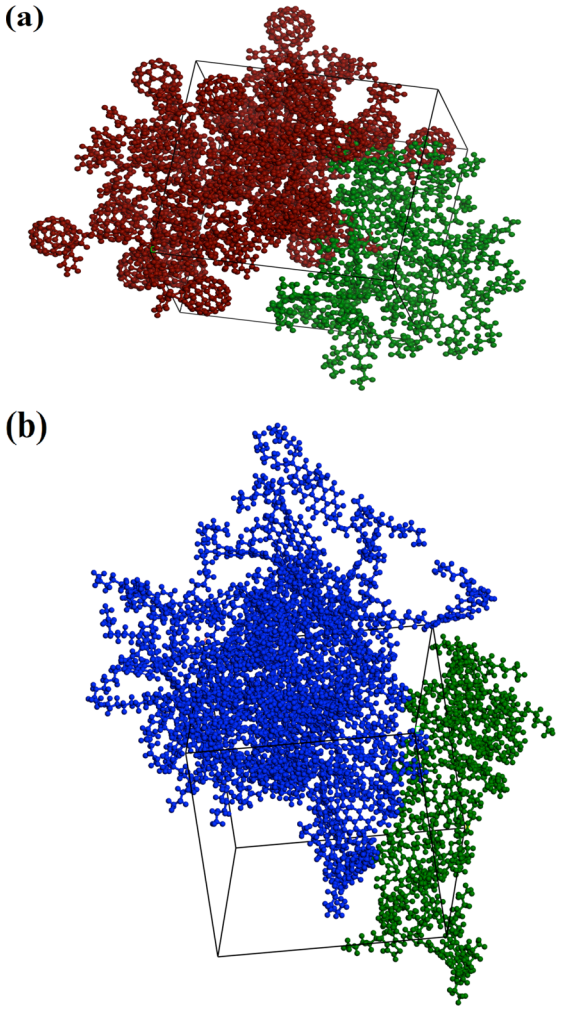

Figure 3. Amorphous cells of (a) P3HT and poly(S_8A_2)-C_{60} blend with d = 1.173 g cm^{-3}, (b) P3HT and PPerAcr blend with d = 1.020 g cm^{-3}.

Table 1. Calculated Polymer–Polymer χ Parameters

	T (K)	P3HT volume fraction	ΔE_{mix} (kcal/mol)	polymer–polymer χ parameter
P3HT-*b*-PPerAcr	500	0.2133	54	322
	550	0.2175	44	236
	600	0.2176	37	184
	650	0.2210	18	81
P3HT-*b*-poly(S_8A_2)-C_{60}	500	0.2696	1245	6366
	550	0.2732	1252	5772
	600	0.2751	1235	5194
	650	0.2801	1188	4562

Velocity Verlet integrator is used to solve Newtonian equations of motion with a time step of 1 fs. The cutoff radius for van der Waals interactions is 9.5 Å with 1 Å spline width.

3.3. Model Materials. P3HT is the acronym of poly(3-hexylthiophene), whose regioregular form[41] is used in solar cells owing to its superior optoelectronic properties. P3HT has been used as the donor material in BHJ solar cells extensively in recent years.[6,42−44] P3HT is the donor block in both systems that have been studied in the current work.

dx.doi.org/10.1021/am400566f | ACS Appl. Mater. Interfaces 2013, 5, 4617−4624

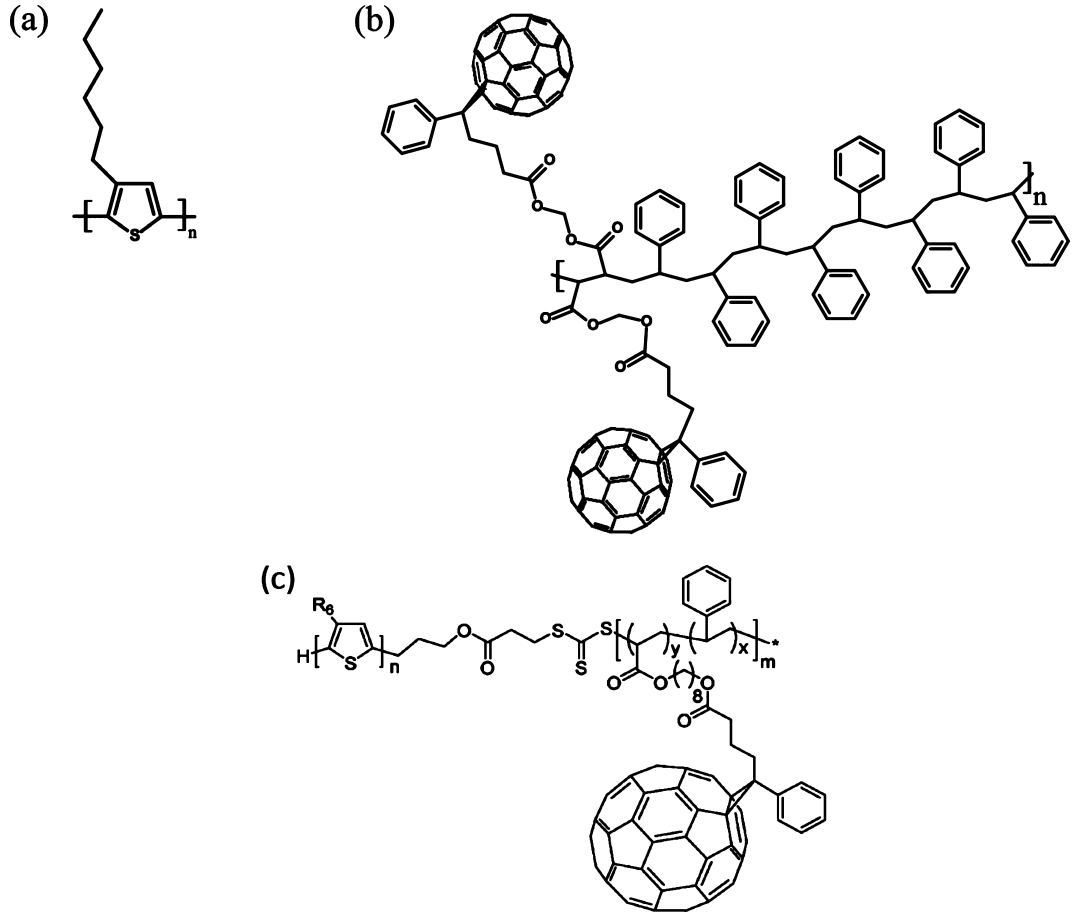

Figure 4. (a) P3HT repeat unit (3-hexylthiophene), (b) Poly(S_8A_2)-C_{60} repeat unit, and (c) P3HT-b-Poly(S_xA_y)-C_{60}.

C_{60} (and C_{70}) derivatives in the form of phenyl-C61-butyric acid methyl ester (PCBM) have been used extensively in the past decade as the acceptor material. Several attempts have been made to synthesize C_{60}-containing blocks to be used in the polymer solar cells.[45−48] One example which is used in our work is Poly(S_xA_y)-C_{60} in which S stands for styrene and A stands for acrylate. Yang et al.[49] fabricated diblock copolymers with different x to y ratios and Poly(S_8A_2)-C_{60} yielded the best performance; hence it is used in the current work as the acceptor block. Figure 4 is the schematic representation of P3HT and Poly(S_8A_2)-C_{60} repeat units and P3HT-b-Poly(S_xA_y)-C_{60}.

P3HT molecule with 40 (3-hexylthiophene) units for which MW = 8316.12 g/mol and poly(S_8A_2)-C_{60} with 10 repeat units for which MW = 29916.9 g/mol are used in the simulations.

Electron transporting small molecules such as derivatives of perylene tetracarboxydiimide (PDI) have been used in PSCs as the acceptor materials. Unlike PCBM which is a weak absorber, perylene derivatives have the advantage of enhanced light absorption in the visible range but solar cells fabricated using these molecules tend to have a very low efficiency[50] because of the formation of microsized PDI crystals due to aggregation. Diblock copolymer fabrication is the best approach to prevent PDI crystal formation. Rajaram et al.[51] fabricated P3HT-b-Poly(n-butyl acrylate-*stat*-acrylate perylene) as a compatibilizer to address this problem. This copolymer (Figure 5) is used for our simulations.

PPerAcr with 40 repeat units for which MW = 33006.1 g/mol is used for simulations.

4. RESULTS AND DISCUSSION

Table 1 in the Supporting Information shows the computed density values of the pure components of the blocks that make up of the diblock copolymers of interest and their binary blends after NPT MD annealings.

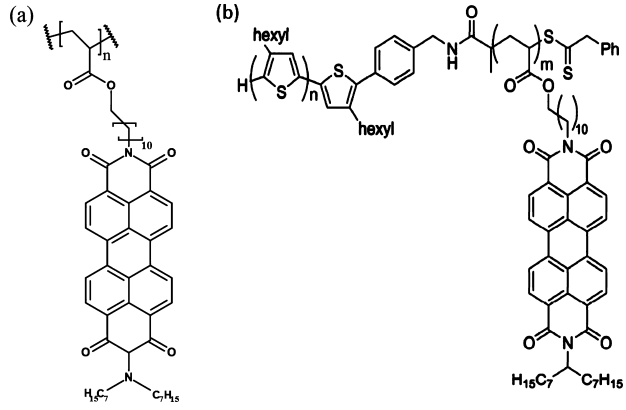

Figure 5. (a) PPerAcr repeat unit and (b) P3HT-b-Poly(n-butyl acrylate-stat-acrylate perylene).

Volume fractions of blocks in the diblock copolymer were then calculated using the density values of the pure blocks and of their molar weights. And the Flory−Huggins interaction parameter was calculated using eq 3.

ΔE_{mix} shown in eq 3 is the difference between the potential energy of binary blends and the corresponding pure homopolymers:

$$\Delta E_{mix} = E_{blend} - E_1 - E_2 \quad (5)$$

The results of such calculations are summarized in Table 2.

Table 1 lists the calculated polymer−polymer χ parameters. However, in order to use diblock copolymer phase diagrams in

dx.doi.org/10.1021/am400566f | ACS Appl. Mater. Interfaces 2013, 5, 4617−4624

Table 2. Calculated segment−segment χ parameters

	T (K)	total cell volume ($cc/mol_{copolymer}$)	lattice site number	segment−segment χ parameter
P3HT-*b*-PPerAcr	500	40504	236.8	1.36
	550	41260	233.9	1.01
	600	41960	232.5	0.79
	650	42746	229.1	0.35
P3HT-*b*-poly(S_8A_2)-C_{60}	500	31766	185.7	34.27
	550	32118	182.1	31.69
	600	32607	180.7	28.75
	650	32942	176.5	25.84

the prediction of the nanomorphology, these values should be converted to the segment−segment χ parameter by dividing them by the total number of lattice sites in the simulation cell. Based on the lattice theory, the volume of each lattice site is considered to be equal to the smaller of segment volumes of the components involved. The total number of sites in the simulation cell can be obtained by dividing the total cell volume by the volume of a P3HT segment. The results are shown in Table 2.

It is obvious that the temperature dependence of the segment−segment χ parameters exhibits the same trend as predicted by eq 2 (see Figures 6 and 7) for both systems, indicating that the pure components would phase segregate at low temperatures.

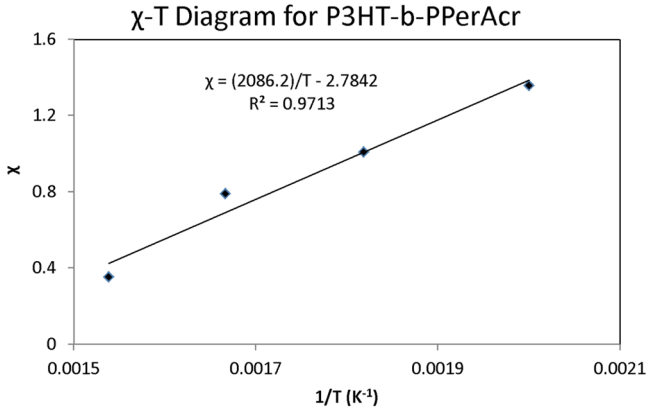

Figure 6. Temperature dependence of χ for P3HT-*b*-PPerAcr.

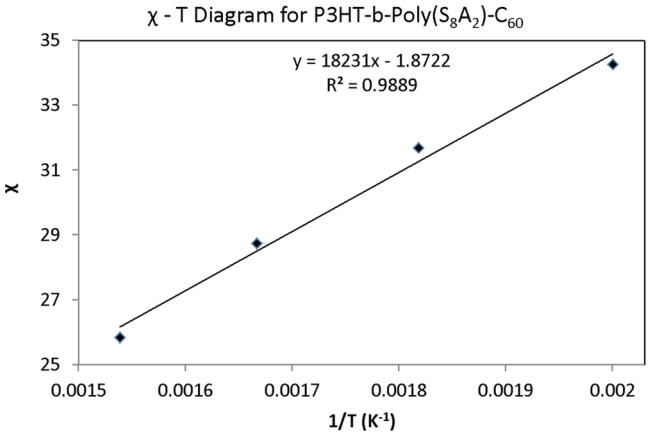

Figure 7. Temperature dependence of χ for P3HT-*b*-poly(S_8A_2)-C_{60}.

The question here is whether the computed segment−segment χ parameters predict the nanomorphology of the diblock copolymers. To evaluate the effectiveness of MD simulations as a prognostication tool, a comparison will be made between predictions of the MD simulation results along with the use of the block copolymer theory and AFM images from experimental work. Results from Yang et al.[49] for P3HT-b-Poly(S_8A_2)-C_{60} are used in this comparison.

To predict the phase nanomorphology, the total degrees of polymerization (N) of the diblock copolymers used in the computational studies and volume fraction of each block are needed in addition to the χ parameter. Data provided by Yang et al.[49] are summarized in Table 3.

Table 3. Experimental Data Provided for P3HT-b-Poly(S8A2)-C60 by Yang et al.[49]

3-hexylthiophene mol %	styrene mol %	acrylate mol %	MW (g/mol)
12	71	17	18 500

On the basis of the data in Table 3, further information can be obtained for P3HT-b-Poly(S_8A_2)-C_{60}, which is shown in Table 4.

Table 4. Total Degree of Polymerization and Volume Fractions of the Blocks of System 1

degree of polymerization	13.67
φ_{P3HT}	0.094
$\varphi_{P(S8A2)-C60}$	0.906
χN in 600 K	393

On the basis of the values shown in Table 4 and the assumption that system 1 exhibits similar nanostructures over comparable volume fraction ranges shown in Figure 2, pure P3HT cylinders inside Poly(S_8A_2)-C_{60} phase are expected. AFM image of the P3HT-b-Poly(S_8A_2)-C_{60} phase published by Yang et al.[49] shows formation of P3HT cylindrical boundaries which is consistent with our prediction.

Moreover, the pair distribution functions, $g(r)$, of the pure polymers and their blends validate phase segregation in block copolymers. Figure 8 shows pair distribution functions for hydrogen atoms of P3HT molecule for three cases: pure P3HT, P3HT-PPerAcr mixture and P3HT-Poly(S_8A_2)-C_{60} mixture. In the case of pure P3HT, the intermolecular contribution becomes greater than the intramolecular contribution at distances larger than 5 Å from the designated atom. On the other hand, the intramolecular contribution is dominant in the blend cases. This proves that in the cases of blends, there is a barrier of PPerAcr or Poly(S_8A_2)-C_{60} molecules between P3HT molecules.

On the basis of the above results, we expect that the MD approach can be used to predict the nanomorphology of diblock copolymers used in the active layer of PSCs. Our approach is particularly relevant to the construction of bulk heterojunctions consisting of polymer−polymer blends and ordered small molecule−polymer heterojunctions based on pattern definition using diblock polymers.

As mentioned previously, the ideal architecture for high efficiency consists of an ordered bulk heterojunction with charge percolation pathways for both types of charge carriers and separated donor and acceptor phases of size comparable to their respective exciton diffusion lengths.[52] In pursuit of this

dx.doi.org/10.1021/am400566f | ACS Appl. Mater. Interfaces 2013, 5, 4617−4624

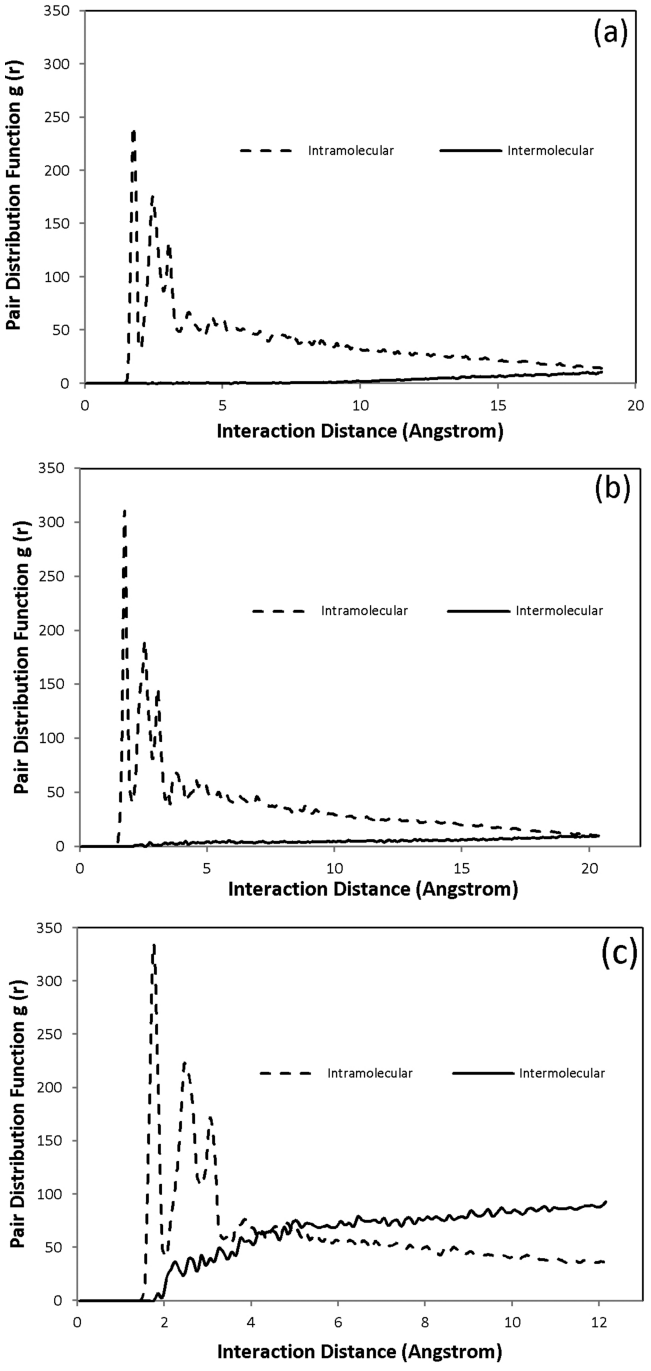

Figure 8. Pair distribution function plots for hydrogen atoms of P3HT in (a) P3HT and poly(S_8A_2)-C_{60} blend, (b) P3HT and PPerAcr blend, (c) pure P3HT.

goal, hybrid solar cells consisting of inorganic n-type large band gap ZnO or TiO_2 nanorod/nanotube arrays filled with a *p*-type semiconducting polymer have attracted much interest.[53] In contrast, all-organic ordered heterojunctions could have simpler processing and can also be designed to absorb light more efficiently by incorporating n-type absorber. However, all-organic ordered heterojunction solar cells have presently not been achieved because of material compatibility issues. For instance, when it is attempted to fill nanorod arrays of a acceptor with a corresponding solution processed donor (or vice versa), the nanorod array architecture softens, buckles, recrystallizes, or otherwise changes its morphology due to the effect of the organic solvent(s) used in the subsequent step.[54] The use of diblock copolymers that vertically phase segregate into cylindrical domains offers a solution to this vexing problem, and allows the construction of ordered heterojunction solar cells. Our work advances the systematic design of such diblock copolymers and highlights the predictive value of molecular dynamics simulations in pretesting the morphology of such diblock copolymer films.

5. CONCLUSION

Three factors are known to control the degree of self-segregation and Nanomorphology of two diblock copolymers: Flory–Huggins interaction parameter (χ), volume fraction of the blocks in the polymer and total degree of polymerization. Molecular dynamics simulations were utilized to calculate the χ parameter for P3HT-b-Poly(S_8A_2)-C_{60} and P3HT-b-PPerAcr thatt are of special interest in the polymer solar cell area. In the first step NPT calculation were performed to find equilibrium density of the system and then NVT simulation were used to calculate potential energy of the system that is required to calculate the χ parameter. In the studied temperature range, χ parameter was shown to have a linear correlation with the reciprocal temperature that is consistent with previous experimental observations. Moreover, strong segregation of block copolymers into cylindrical boundaries is predicted for P3HT-b-Poly(S_8A_2)-C_{60}, which is consistent with AFM images of this copolymer available in the literature.

■ ASSOCIATED CONTENT

Supporting Information

Table of NPT molecular dynamics simulation results. This material is available free of charge via the Internet at http://pubs.acs.org.

■ AUTHOR INFORMATION

Corresponding Author

*E-mail: phillip.choi@ualberta.ca.

Notes

The authors declare no competing financial interest.

■ ACKNOWLEDGMENTS

The authors are grateful for the funding from National Science and Engineering Research Council of Canada. This research has been enabled by the use of WestGrid computing resources, which are funded in part by the Canada Foundation for Innovation, Alberta Innovation and Science, BC Advanced Education, and the participating research institutions. WestGrid equipment is provided by IBM, Hewlett-Packard, and SGI.

■ REFERENCES

(1) Kamat, P. V. *J. Phys. Chem. C.* **2007**, *111*, 2834–2860.
(2) Lewis, N. S. *Science* **2007**, *315*, 798–801.
(3) Coakley, K. M.; McGehee, M. D. *Chem. Mater.* **2004**, *16*, 4533–4542.
(4) Markov, D. E.; Amsterdam, E.; Blom, P. W. M.; Sieval, A. B.; Hummelen, J. C. *J. Phys. Chem. A* **2005**, *109*, 5266–5274.
(5) Chen, F. C.; Wu, J. L.; Yang, S. S.; Hsieh, K. H.; Chen, W. C. *J. Appl. Phys.* **2008**, *103*, 81–85.
(6) Li, G.; Shrotriya, V.; Huang, J. S.; Yao, Y.; Moriarty, T.; Emery, K.; Yang, Y. *Nat. Mater.* **2005**, *4*, 864–868.
(7) Ma, W. L.; Yang, C. Y.; Gong, X.; Lee, K.; Heeger, A. J. *Adv. Funct. Mater.* **2005**, *15*, 1617–1622.

(8) Vanlaeke, P.; Swinnen, A.; Haeldermans, I.; Vanhoyland, G.; Aernouts, T.; Cheyns, D.; Deibel, C.; D'Haen, J.; Heremans, P.; Poortmans, J.; Manca, J. V. *Sol. Energy Mater. Sol. Cells* **2006**, *90*, 2150−2158.
(9) Swinnen, A.; Haeldermans, I.; Vande Ven, M.; D'Haen, J.; Vanhoyland, G.; Aresu, S.; D'Olieslaeger, M.; Manca, J. *Adv. Funct. Mater.* **2006**, *16*, 760−765.
(10) Li, G.; Yao, Y.; Yang, H.; Shrotriya, V.; Yang, G.; Yang, Y. *Adv. Funct. Mater.* **2007**, *17*, 1636−1644.
(11) Bagui, A.; Iyer, S. S. K. *IEEE Trans. Electron Devices* **2011**, *58*, 4061−4066.
(12) Peet, J.; Kim, J. Y.; Coates, N. E.; Ma, W. L.; Moses, D.; Heeger, A. J.; Bazan, G. C. *Nat. Mater.* **2007**, *6*, 497−500.
(13) Bechara, R.; Leclerc, N.; AĹvque, P.; Richard, F.; Heiser, T.; Hadziioannou, G. *Appl. Phys. Lett.* **2008**, *93*, 66−70.
(14) Bates, F. S.; Fredrickson, G. H. *Annu. Rev. Phys. Chem.* **1990**, *41*, 525−57.
(15) Hoppe, H.; Glatzel, T.; Niggemann, M.; Schwinger, W.; Schaeffler, F.; Hinsch, A.; Lux-Steiner, M. C.; Sariciftci, N. S. *Thin Solid Films* **2006**, *511*, 587−592.
(16) Hoppe, H.; Niggemann, M.; Winder, C.; Kraut, J.; Hiesgen, R.; Hinsch, A.; Meissner, D.; Sariciftci, N. S. *Adv. Funct. Mater.* **2004**, *14* (10), 1005−1011.
(17) Hoppe, H.; Sariciftci, N. S. *J. Mater. Chem.* **2006**, *16* (1), 45−61.
(18) Hoppe, H.; Sariciftci, N. S. Polymer Solar Cells. In *Photoresponsive Polymers II*; Marder, S. R., Lee, K. S., Eds.; Springer: New York, 2008; Vol. *214*; pp 1−86.
(19) Moons, E. *J. Phys.: Condens. Matter* **2002**, *14* (47), 12235−12260.
(20) Nguyen, L. H.; Hoppe, H.; Erb, T.; Gunes, S.; Gobsch, G.; Sariciftci, N. S. *Adv. Funct. Mater.* **2007**, *17* (7), 1071−1078.
(21) van Bavel, S. S.; Barenklau, M.; de With, G.; Hoppe, H.; Loos, J. *Adv. Funct. Mater.* **2010**, *20* (9), 1458−1463.
(22) Do, K.; Huang, D. M.; Faller, R.; Moulé, A. *J. Phys. Chem. Chem. Phys.* **2010**, *12*, 14735−14739.
(23) Lee, C.; Pao, C.; Chu, C. *Energy Environ. Sci* **2011**, *4*, 4124−4132.
(24) Hall, C. K.; Helfand, E. *J. Chem. Phys.* **1982**, *77*, 3275−3282.
(25) Krigbaum, W. R.; Yazgan, S.; Tolbert, W. R. *J. Polym. Sci. Part A-2: Polym. Phys.* **1973**, *11*, 511−527.
(26) Owens, J. N.; Gancarz, I. S.; Koberstein, J. T.; Russell, T. P. *Macromolecules* **1989**, *22*, 3380−3387.
(27) Cohen, R. E.; Ramos, A. R. *Macromolecules* **1979**, *12*, 131−134.
(28) Fredrickson, G. H.; Bates, F. S. *Annu. Rev. Mater. Sci.* **1996**, *26*, 501−550.
(29) Olemskoi, A.; Savelyev, A. *Phys. Rep.* **2005**, *419*, 145−205.
(30) Rosedale, J. H.; Bates, F. S.; Almdal, K.; Mortensen, K.; Wignall, G. D. *Macromolecules* **1995**, *28*, 1429−1443.
(31) Fredrickson, G. H.; Helfand, E. *J. Chem. Phys.* **1987**, *87*, 697−705.
(32) Khandpur, A. K.; Förster, S.; Bates, F. S.; Hamley, I. W.; Ryan, A. J.; Bras, W.; Almdal, K.; Mortensen, K. *Macromolecules* **1995**, *28*, 8796−8806.
(33) Patel, S.; Lavasanifar, A.; Choi, P. *Biomacromolecules* **2008**, *9*, 3014−3023.
(34) Flory, P. J. *Principles of Polymer Chemistry*; Cornell University Press: New York, 1953.
(35) Sun, H. *J. Phys. Chem. B* **1998**, *102*, 7338−7364.
(36) Sagui, C.; Darden, T. A. *Annu. Rev. Biophys. Biomol. Struct.* **1999**, *28*, 155−179.
(37) Flory, P. J. *Macromolecules* **1974**, *7*, 381−392.
(38) Mattice, W. L.; Suter, U. W. *Conformational Theory of Large Molecules: The Rotational Isomeric State Model in Macromolecular Systems*; Wiley: New York, 1994.
(39) Flory, P. J. *Statistical Mechanics of Chain Molecules*; Interscience: New York, 1969.
(40) Berendsen, H. J. C.; Postma, J. P. M.; Van Gunsteren, W. F.; Dinola, A.; Haak, J. R. *J. Chem. Phys.* **1984**, *81*, 3684−3690.
(41) Kim, Y.; Cook, S.; Tuladhar, S. M.; Choulis, S. A.; Nelson, J.; Durrant, J. R.; Bradley, D. D. C.; Giles, M.; Mcculloch, I.; Ha, C. S.; Ree, M. *Nat. Mater.* **2006**, *5*, 197−203.
(42) Reyes-Reyes, M.; Kim, K.; Carroll, D. L. *Appl. Phys. Lett.* **2005**, *87*, 1−3.
(43) Kim, Y.; Choulis, S. A.; Nelson, J.; Bradley, D. D. C.; Cook, S.; Durrant, J. R. *Appl. Phys. Lett.* **2005**, *86*, 1−3.
(44) Padinger, F.; Rittberger, R. S.; Sariciftci, N. S. *Adv. Funct. Mater.* **2003**, *13*, 85−88.
(45) Van Der Veen, M. H.; De Boer, B.; Stalmach, U.; Van De Wetering, K. I.; Hadziioannou, G. *Macromolecules* **2004**, *37*, 3673−3684.
(46) Stalmach, U.; De Boer, B.; Videlot, C.; Van Hutten, P. F.; Hadziioannou, G. *J. Am. Chem. Soc.* **2000**, *122*, 5464−5472.
(47) Barrau, S.; Heiser, T.; Richard, F.; Brochon, C.; Ngov, C.; Van De Wetering, K.; Hadziioannou, G.; Anokhin, D. V.; Ivanov, D. A. *Macromolecules* **2008**, *41*, 2701−2710.
(48) De Boer, B.; Stalmach, U.; Van Hutten, P. F.; Melzer, C.; Krasnikov, V. V.; Hadziioannou, G. *Polymer* **2001**, *42*, 9097−9109.
(49) Yang, C.; Lee, J. K.; Heeger, A. J.; Wudl, F. *J. Mater. Chem.* **2009**, *19*, 5416−5423.
(50) Li, J.; Dierschke, F.; Wu, J.; Grimsdale, A. C.; Müllen, K. *J. Mater. Chem.* **2006**, *16*, 96−100.
(51) Rajaram, S.; Armstrong, P. B.; Bumjoon; Kim, J.; Fréchet, J. M. J. *Chem. Mater.* **2009**, *21*, 1775−1777.
(52) Coakley, K. M.; Liu, Y. X.; Goh, C.; McGehee, M. D. *MRS Bull.* **2005**, *30*, 37−40.
(53) Shankar, K.; Mor, G. K.; Paulose, M.; Varghese, O. K.; Grimes, C. A. *J. Non-Cryst. Solids* **2008**, *354*, 2767−2771.
(54) Van Dijken, J. G.; Fleischauer, M. D.; Brett, M. J. *Org. Electron.* **2011**, *12*, 2111−2119.